Radiology

ORIGINAL RESEARCH • NEURORADIOLOGY

Multicenter Evaluation of AI-generated DIR and PSIR for Cortical and Juxtacortical Multiple Sclerosis Lesion Detection

Piet M. Bouman, PhD • Samantha Noteboom, MSc • Fernando A. Nobrega Santos, PhD • Erin S. Beck, PhD • Gregory Bliault, MSc • Marco Castellaro, PhD • Massimiliano Calabrese, PhD • Declan T. Chard, PhD • Paul Eichinger, PhD • Massimo Filippi, PhD • Matilde Inglese, PhD • Caterina Lapucci, PhD • Andrzej Marciniak, PhD • Bastiaan Moraal, PhD • Alfredo Morales Pinzon, PhD • Mark Mühlau, PhD • Paolo Preziosa, PhD • Daniel S. Reich, PhD • Maria A. Rocca, PhD • Menno M. Schoonheim, PhD • Jos W. R. Twisk, PhD • Benedict Wiestler, PhD • Laura E. Jonkman, PhD • Charles R. G. Guttmann, PhD • Jeroen J. G. Geurts, PhD • Martijn D. Steenwijk, PhD

From the MS Center Amsterdam, Anatomy & Neurosciences, Amsterdam Neuroscience, Amsterdam UMC, Vrije Universiteit Amsterdam, De Boelelaan 1117, Amsterdam, the Netherlands (P.M.B., S.N., F.A.N.S., M.M.S., J.J.G.G., M.D.S.); Translational Neuroradiology Section, National Institute of Neurological Disorders and Stroke, National Institutes of Health, Bethesda, Md (E.S.B., D.S.R.); Department of Neurology, Icahn School of Medicine at Mount Sinai, New York, NY (E.S.B.); Bio-imaging Institute, University of Bordeaux, Bordeaux, France (G.B.); Neurology Section, Department of Neuroscience, Biomedicine and Movement Sciences, University of Verona, Verona, Italy (M. Castellaro, M. Calabrese); Department of Information Engineering, University of Padova, Padova, Italy (M. Castellaro); NMR Research Unit, Queen Square MS Centre, Department of Neuroinflammation, UCL Queen Square Institute of Neurology, Faculty of Brain Sciences, University College London, London, UK (D.T.C.); National Institute for Health Research University College London Hospitals Biomedical Research Centre, London, UK (D.T.C.); Departments of Neuroradiology (P.E., B.W.) and Neurology (M.M.), School of Medicine, Klinikum Rechts der Isar, Technical University of Munich, Munich, Germany; Neuroimaging Research Unit, Division of Neuroscience Neurology Unit, IRCCS San Raffaele Scientific Institute Vita-Salute San Raffaele University, Milan, Italy (M.F., P.P., M.A.R.); Department of Neuroscience, Rehabilitation, Ophthalmology, Genetics, Maternal and Child Health, University of Genova, Genoa, Italy (M.I., C.L.); IRCCS Ospedale Policlinico San Martino, Largo Rosanna Benzi, Genoa, Italy (M.I., C.L.); Center for Neurologic Imaging, Department of Radiology, Brigham and Women's Hospital, Harvard Medical School, Boston, Mass (A.M., A.M.P., C.R.G.G.); Department of Radiology and Nuclear Medicine, MS Center Amsterdam, Amsterdam Neurosciences, Amsterdam UMC, Vrije Universiteit Amsterdam, Amsterdam, the Netherlands (B.M.); Department of Epidemiology and Data Science, Amsterdam University Medical Center, Amsterdam, the Netherlands (J.W.R.T.); Anatomy & Neurosciences, Amsterdam UMC, Vrije Universiteit Amsterdam, Amsterdam, the Netherlands (L.E.J.); and Amsterdam Neuroscience, Brain Imaging and Neurodegeneration, Amsterdam, the Netherlands (L.E.J.). Received June 7, 2022; revision requested August 11; revision received November 18; accepted November 28. **Address correspondence to** P.M.B. (email: *p.bouman@amsterdamumc.nl*).

Supported by Stichting MS Research (Dutch MS Research Foundation) (grant 19-049). Development of the SPINE platform was supported in part by the International Progressive MS Alliance (award reference number PA-1603-08175), as well as the Bordeaux University Foundation through donations from Roche Pharmaceuticals and Talan.

Conflicts of interest are listed at the end of this article.

See also the editorial by Zivadinov and Dwyer in this issue.

Radiology 2023; 307(2):e221425 • https://doi.org/10.1148/radiol.221425 • Content codes: NR AI MR

Background: Cortical multiple sclerosis lesions are clinically relevant but inconspicuous at conventional clinical MRI. Double inversion recovery (DIR) and phase-sensitive inversion recovery (PSIR) are more sensitive but often unavailable. In the past 2 years, artificial intelligence (AI) was used to generate DIR and PSIR from standard clinical sequences (eg, T1-weighted, T2-weighted, and fluid-attenuated inversion-recovery sequences), but multicenter validation is crucial for further implementation.

Purpose: To evaluate cortical and juxtacortical multiple sclerosis lesion detection for diagnostic and disease monitoring purposes on AI-generated DIR and PSIR images compared with MRI-acquired DIR and PSIR images in a multicenter setting.

Materials and Methods: Generative adversarial networks were used to generate AI-based DIR (n = 50) and PSIR (n = 43) images. The number of detected lesions between AI-generated images and MRI-acquired (reference) images was compared by randomized blinded scoring by seven readers (all with >10 years of experience in lesion assessment). Reliability was expressed as the intraclass correlation coefficient (ICC). Differences in lesion subtype were determined using Wilcoxon signed-rank tests.

Results: MRI scans of 202 patients with multiple sclerosis (mean age, 46 years ± 11 [SD]; 127 women) were retrospectively collected from seven centers (February 2020 to January 2021). In total, 1154 lesions were detected on AI-generated DIR images versus 855 on MRI-acquired DIR images (mean difference per reader, 35.0% ± 22.8; P < .001). On AI-generated PSIR images, 803 lesions were detected versus 814 on MRI-acquired PSIR images (98.9% ± 19.4; P = .87). Reliability was good for both DIR (ICC, 0.81) and PSIR (ICC, 0.75) across centers. Regionally, more juxtacortical lesions were detected on AI-generated DIR images than on MRI-acquired DIR images (495 [42.9%] vs 338 [39.5%]; P < .001). On AI-generated PSIR images, fewer juxtacortical lesions were detected than on MRI-acquired PSIR images (232 [28.9%] vs 282 [34.6%]; P = .02).

Conclusion: Artificial intelligence–generated double inversion-recovery and phase-sensitive inversion-recovery images performed well compared with their MRI-acquired counterparts and can be considered reliable in a multicenter setting, with good between-reader and between-center interpretative agreement.

Supplemental material is available for this article.

Multiple sclerosis is an inflammatory, demyelinating, and neurodegenerative disease of the central nervous system that leads to a variety of physical and cognitive disabilities (1–3). Although multiple sclerosis lesions can affect the entire central nervous system, they are most conspicuous in the white matter at MRI (4–6). However, immunohistochemical staining revealed that multiple sclerosis lesions also frequently occur in the cortical gray

Abbreviations

AI = artificial intelligence, DIR = double inversion recovery, ICC = intraclass correlation coefficient, PSIR = phase-sensitive inversion recovery

Summary

Artificial double inversion-recovery and phase-sensitive inversion-recovery MRI scans were generated from multicenter input data, with high between-center and between-reader reliability for detection of cortical and juxtacortical multiple sclerosis lesions.

Key Results

- In a retrospective study of 202 patients with multiple sclerosis, readers could detect more lesions on artificially generated than on MRI-acquired double inversion-recovery (DIR) images (1154 vs 855; $P = .02$).
- Cortical lesions could be detected at artificial MRI, with high between-center (intraclass correlation coefficient [ICC] of 0.81 for DIR and 0.75 for phase-sensitive inversion recovery [PSIR]) and between-reader reliability (ICC of 0.76 for DIR and 0.85 for PSIR).

matter (7). Cortical gray matter lesions are known to be related to disability and cognition and could thus play an important role in monitoring disease progression in patients with multiple sclerosis (8–10). Cortical gray matter lesions visible at MRI were found to be a pathologic hallmark for multiple sclerosis, which has led to expansion of the diagnostic criteria from only juxtacortical lesions (ie, touching the cortex) to lesions that are juxtacortical *or* cortical (11).

Due to their small size and low contrast relative to normal-appearing gray matter, cortical lesions are inconspicuous on images acquired with conventional clinical MRI sequences (eg, T1-weighted, T2-weighted, and fluid-attenuated inversion-recovery, or FLAIR, sequences) (12). Improved visualization of cortical lesions has been achieved with the development of advanced MRI techniques, such as double inversion-recovery (DIR) and phase-sensitive inversion-recovery (PSIR) sequences (4,5,7,13,14). However, these sequences are largely absent in routine diagnostic and clinical trial evaluation protocols due to their substantial acquisition times (ie, 10–15 minutes). Pilot studies using artificial intelligence (AI) have recently enabled the generation of artificial DIR images from routine clinical MRI protocols (ie, combinations of T1- and proton density–/T2-weighted sequences) (15,16). Histopathologic validation of AI-generated DIR images vis-à-vis MRI-acquired images showed equal sensitivity and specificity values (17). To leverage the potential of AI-generated DIR and PSIR images to serve as an alternative to MRI-acquired DIR and PSIR images, multicenter data evaluation is crucial for understanding their value in a clinical or research setting with hardware and sequence parametrization variability.

The primary aim of our study was to evaluate cortical and juxtacortical multiple sclerosis lesion detection for diagnostic and disease monitoring purposes on AI-generated DIR and PSIR images compared with MRI-acquired DIR and PSIR images in a multicenter setting.

Materials and Methods

Study Design and Participants

Data for our study were retrospectively collected between February 2020 and January 2021 from seven academic medical centers (National Institutes of Health, United States; University College London, United Kingdom; Technical University of Munich, Germany; University of Genoa, Italy; IRCCS San Raffaele Scientific Institute, Italy; Università di Verona, Italy; and Amsterdam UMC, the Netherlands). Some of the data were previously analyzed for different purposes (Appendix S1). All patients provided written informed consent before study commencement and data sharing. Studies were approved by the institutional ethics review boards of all participating centers.

Collection of MRI Data

Each participating center was requested to provide whole-brain MRI data of at least 20 patients diagnosed with multiple scle-

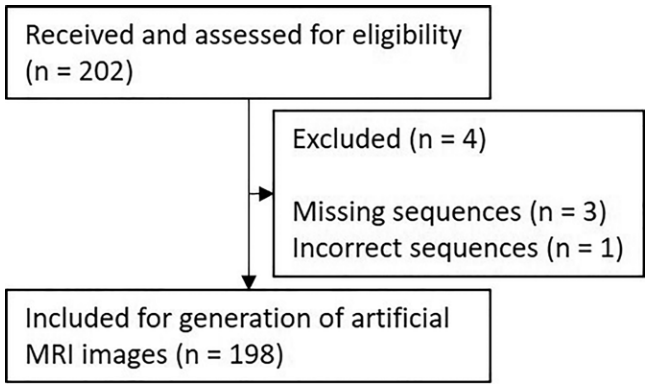

Figure 1: Flowchart of included and excluded patients displays number of patients from whom images were received and reasons for exclusion.

Table 1: Patient Demographics and Disease Characteristics

	DIR Subset (n = 160)		PSIR Subset (n = 125)	
Parameter	Women	Men	Women	Men
No. of patients*	98 (61.3)	62 (38.7)	87 (69.6)	38 (30.4)
Age (y)	50 ± 10	48 ± 10	43 ± 11	43 ± 11
Age range (y)	20–66	29–66	20–66	20–66
Disease type†				
RR	52	22	73	26
SP	30	18	11	6
PP	16	22	3	6
Disease duration (y)	14.7 ± 10.3	12.8 ± 7.7	10.1 ± 8.7	10.7 ± 7.1
EDSS score‡	4 (0–8)	5 (0–8)	2 (0–7)	3.5 (0–8)

Note.—Unless stated otherwise, data are means ± SDs. DIR = double inversion recovery, EDSS = Expanded Disability Status Scale, PP = primary progressive multiple sclerosis, PSIR = phase-sensitive inversion recovery, RR = relapsing-remitting multiple sclerosis, SP = secondary progressive multiple sclerosis.

* Data in parentheses are percentages.

† Data are numbers of patients.

‡ Data are medians, with ranges in parentheses.

rosis according to McDonald or Poser criteria (11,18,19). Inclusion and exclusion criteria were presence or absence of MRI scans acquired at clinical field strength of 1.5 T or 3.0 T, including a DIR and/or PSIR sequence (ideally three-dimensional, near 1-mm isotropic resolution), a three-dimensional T1-weighted sequence (near 1-mm isotropic resolution), and either a proton density–/T2-weighted sequence, fluid-attenuated inversion-recovery sequence, or both (3-mm sections or higher resolution). Imaging parameters are displayed in Appendix S2 (Tables S1–S5).

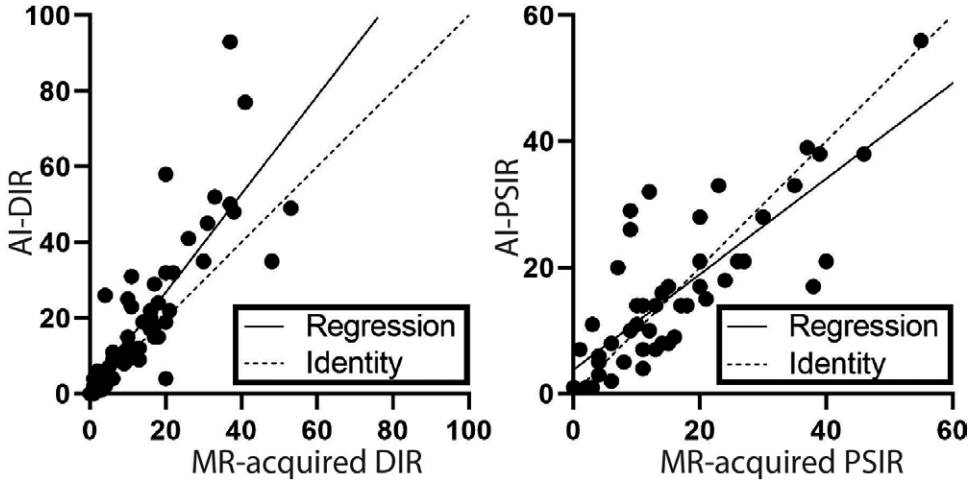

Figure 2: Graphical overview of detected cortical and juxtacortical lesions on artificial intelligence (AI)–generated versus MRI-acquired images. Line graphs show AI-generated double inversion-recovery (DIR) images vis-à-vis MRI-acquired DIR images per patient (left) and AI-generated phase-sensitive inversion-recovery images (PSIR) vis-à-vis MRI-acquired PSIR images (right). The solid line indicates the regression, and the dashed line indicates identity.

Image Preprocessing and Generation of Artificial Images

An extensive description of the full image processing pipeline is provided elsewhere (15). In brief, all available contrasts of each patient were coregistered with each other with use of rigid body transformation using FLIRT (liner image registration tool, part of the Functional MRI of the Brain Software Library, or FSL, version 5.0.4; *http://fsl.fmrib.ox.ac.uk*). The resulting transformation matrixes were used to rigidly transform the data of all individuals into 1-mm Montreal Neurological Institute system standard space (spline interpolation). The skull was removed from the data by using bet-premask (FSL). Variance scaling, but not any other intensity or bias field correction, was applied to each individual contrast in each patient.

Next, two separate generative adversarial networks (U-Net–like convolutional networks) were trained to generate either artificial DIR or PSIR images from the available clinical MRI sequences (ie, T1-weighted and proton density–/T2-weighted or fluid-attenuated inversion-recovery sequences). Images from the different centers were equally distributed into training and test sets (2:1 ratio), after which the generative adversarial networks were applied to the training sets. The code that was used to generate the artificial images is deposited at *https://github.com/MrtnStnwk/DeepContrast*.

Lesion Identification

AI-generated DIR and PSIR images, along with their MRI-acquired counterparts, were randomly distributed for lesion assessment among seven readers, all from different centers. Each reader received 30 data sets: eight AI-generated DIR images, seven AI-generated PSIR images, and the corresponding MRI-acquired images. One randomly selected DIR and one randomly selected PSIR data set were provided to all readers for reliability calculations. The other data sets were reviewed by only one reader. Images were provided in random order and randomly left-right flipped to reduce recognition probability. Lesion detection was performed by seven authors (B.M., C.L., D.T.C., E.S.B., M.M., P.E., and P.P., all with >10 years of experience in cortical lesion detection) in accordance with consensus recommendations by the Magnetic Resonance Imaging in MS, or MAGNIMS, group for MRI-acquired as well as AI-generated DIR images and sequence-specific guidelines for MRI-acquired and AI-generated PSIR images (14,20). Readers were also asked to indicate lesion type as juxtacortical (touching but not entering cortical gray matter), leukocortical (situated in part in the cortex and in part in the adjacent white matter), intracortical (fully situated in the cortex), or infratentorial (below the cerebellar tentorium). In-depth descriptions of the procedures and lesion detection criteria are provided in Appendixes S3–S5.

Statistical Analysis

The number of lesions detected on the AI-generated images was compared with that on the corresponding MRI-acquired images, using the latter as reference. Distribution of the data was assessed for normality with use of Kolmogorov-Smirnov tests and log-transformed if not normally distributed.

Statistical analyses were performed by three authors (P.M.B., L.E.J., and J.W.R.T., with 4, 8, and >15 years of experience, respectively). Differences in the number of detected lesions per patient were assessed using pairwise *t* tests, and differences in the number of detected lesions at the lesion subtype level were assessed using pairwise Wilcoxon signed-rank tests. Between-reader agreement (reliability; identical patient) was assessed by calculating the intraclass correlation coefficient (ICC) (two-way mixed model with absolute agreement). Calculations were based on the number of lesions identified per 20 sections (ie, 0–20; 21–40; 41–60; 60–80). Using a similar model, reliability between AI-generated and MRI-acquired DIR and PSIR images across all centers (nonidentical patients) was determined.

Post hoc precision of the AI-generated images was estimated using data from five randomly selected patients per contrast. Lesions detected on AI-generated and MRI-acquired images were matched to obtain true- and false-positive results (taking

MRI-acquired images as the reference). This allowed the calculation of precision (precision = true-positive results divided by total positive results; performed by P.M.B.). Additionally, image contrast ratios were calculated for a random subsample of 14 patients to explore the origin of differences. A detailed description of these calculations is provided in Appendix S6. $P < .05$ was considered indicative of statistically significant difference.

Analyses were performed using Statistical Package for Social Sciences, version 28.0 (IBM).

Results

Patient Characteristics

DIR images ($n = 160$) and PSIR images ($n = 125$) from a total of 202 patients with multiple sclerosis (mean age, 46 years ± 11 [SD]; 127 women) were received. Data from four patients were excluded due to missing or incorrect sequences. The training and test sets consisted of 106 and 50 patients, respectively, for DIR and 82 and 43 patients, respectively, for PSIR sequences. A flowchart of the procedure is displayed in Figure 1. The demographic characteristics of the patients for the DIR and PSIR training and test sets are displayed in Table 1.

Lesion Detection on AI-generated Images

An overview of the number of lesions that were detected on AI-generated versus MRI-acquired DIR and PSIR images is provided in Figure 2.

On AI-generated DIR images, a total of 1154 lesions were detected, compared with 855 on MRI-acquired DIR images. Some examples of cortical lesions that were detected on AI-generated and MRI-acquired DIR images are depicted in Figure 3. Averaged over patients, the readers detected 35% more lesions on AI-generated DIR images than on MRI-acquired DIR images, with differences ranging from 15% to 79% more lesions ($t = 2.39$, $P = .02$). The median number of detected lesions was 15 (IQR, 8–23) for AI-generated DIR and 13 (IQR, 6–20) for MRI-acquired DIR images. Reliability analysis between centers showed good agreement in the number of detected lesions on AI-generated and MRI-acquired DIR images across all assessed data sets (ICC, 0.81 [95% CI: 0.68, 0.89]). The precision of the AI-generated DIR images was 72.8% ± 13.1. An example of a lesion that appears juxtacortical on the AI-generated DIR image but subcortical (and thus a false-positive finding, as readers were specifically instructed not to mark subcortical lesions) on the MRI-acquired DIR image is presented in Figure 4.

For PSIR, a total of 803 lesions were detected on AI-generated images and 814 on MRI-acquired images. Examples of cortical lesions that were detected on AI-generated and MRI-acquired PSIR images are depicted in Figure 5. The overall number of lesions detected on AI-generated PSIR images compared with MRI-acquired PSIR images was 98.9% ± 19.4, ranging from 71.6% to 116.8% for the different readers ($t = -0.16$, $P = .87$). The median number of detected lesions was 14 (IQR, 7–21) for AI-generated PSIR images and 13 (IQR, 7–22) for MRI-acquired PSIR images. Reliability analysis between centers for AI-generated PSIR images versus MRI-acquired PSIR images showed good agreement for the number of detected lesions across all assessed data sets (ICC, 0.75 [95% CI: 0.59, 0.85]). The precision of the AI-generated PSIR images was 69.5% ± 13.1.

Assessment of between-reader variability (same data set for all readers) showed good agreement for AI-generated DIR images (ICC, 0.76 [95% CI: 0.43, 0.98]), MRI-acquired DIR images (ICC, 0.85 [95% CI: 0.58, 0.99]), AI-generated PSIR images (ICC, 0.85 [95% CI: 0.59, 0.99]), and MRI-acquired PSIR images (ICC, 0.85 [95% CI: 0.59, 0.99]). The median number of lesions detected in the patient whose images were assessed by all readers was 15 (IQR, 11–22) for AI-generated DIR, 12 (IQR, 11–15) for MRI-acquired DIR, eight (IQR, five to eight) for AI-generated PSIR, and seven (IQR, five to nine) for MRI-acquired PSIR.

Differences between Identified Lesion Subtypes on Different Sequences

A graphical overview of the detected differences between lesion subtypes on AI-generated versus MRI-acquired images is depicted in Figure 6. For AI-generated versus MRI-acquired DIR images, respectively, 495 of 1154 (42.9%) and 338 of 855 (39.5%) detected lesions were classified as juxtacortical ($Z = 3.52$, $P < .001$); 316 of 1154 (27.4%) and 261 of 855 (30.5%) as leukocortical ($Z = -1.38$, $P = .17$); 92 of 1154 (8.0%) and 119 of 855 (13.9%) as intracortical ($Z = -1.52$, $P = .13$); and 248 of 1154 (21.5%) and 128 of 855 (15.0%) as infratentorial ($Z = -4.30$, $P < .001$). Three of 1154 lesions (0.3%) and nine of 855 lesions (1.1%) were not classified by the reader.

For AI-generated versus MRI-acquired PSIR images, respectively, the majority of lesions were classified as leukocortical: 282 of 803 (35.1%) and 308 of 814 (37.8%) ($Z = -0.87$, $P = .38$); followed by juxtacortical lesions: 232 of 803 (28.9%) and 282 of 814 (34.6%) ($Z = -2.42$, $P = .02$); intracortical lesions: 97 of 803 (12.1%) and 116 of 814 (14.3%) ($Z = -1.53$, $P = .13$); and infratentorial lesions: 184 of 803 (22.9%) and 99 of 814 (12.2%) ($Z = -3.37$, $P = .001$). Eight of 803 lesions (1.0%) and nine of 814 lesions (1.1%) were not classified by the reader.

Image Contrast Ratios

Contrast ratios were calculated for a random subset of 28 lesions that were detected by the readers in 14 different patients. The outcomes of the contrast ratio calculations (calculated for 28 regions) are presented in Table 2. For AI-generated versus MRI-acquired DIR images, no differences in cortical lesion versus normal-appearing gray matter contrast (0.23 ± 0.20 vs 0.26 ± 0.23, respectively; $Z = -1.94$, $P = .053$) were observed, but the contrast was higher for normal-appearing gray matter versus normal-appearing white matter in the MRI-acquired DIR images (0.43 ± 0.16 vs 0.51 ± 0.18; $Z = -3.26$, $P = .001$). For PSIR, contrast between cortical lesions versus normal-appearing gray matter was higher in MRI-acquired images (–0.08 ± 0.12 vs –0.12 ± 0.07; $Z = -3.17$, $P = .002$), and no evidence of a difference was found for the contrast ratio of normal-appearing gray matter versus normal-appearing white matter (–0.12 ± 0.08 vs –0.13 ± 0.08; $Z = -1.07$, $P = .29$).

Discussion

Our study investigated whether otherwise inconspicuous cortical or juxtacortical multiple sclerosis lesions can be detected on

artificial intelligence (AI)–generated double inversion-recovery (DIR) and phase-sensitive inversion-recovery (PSIR) images in a multicenter data set. An earlier study in a single-center setting using 1.5-T MRI showed that AI could potentially mitigate the issue of often-absent DIR sequences in clinical care and clinical trials (15). Our results demonstrate that more lesions can be detected on AI-generated DIR images than on their MRI-acquired counterparts (t = 2.39, P = .02) and an equal number of lesions on the AI-generated PSIR images as on their MRI-acquired counterparts (t = –0.16, P = .87), with good between-center (intraclass correlation coefficient [ICC], 0.81 and 0.75 for DIR and PSIR, respectively) and between-reader agreement (ICC, 0.76 and 0.85 for AI-generated and MRI-acquired DIR images, respectively, and 0.85 and 0.85 for AI-generated and MRI-acquired PSIR images). These results suggest that AI-generated DIR and PSIR images could be used in diagnostic and disease monitoring settings when MRI-acquired sequences are not available.

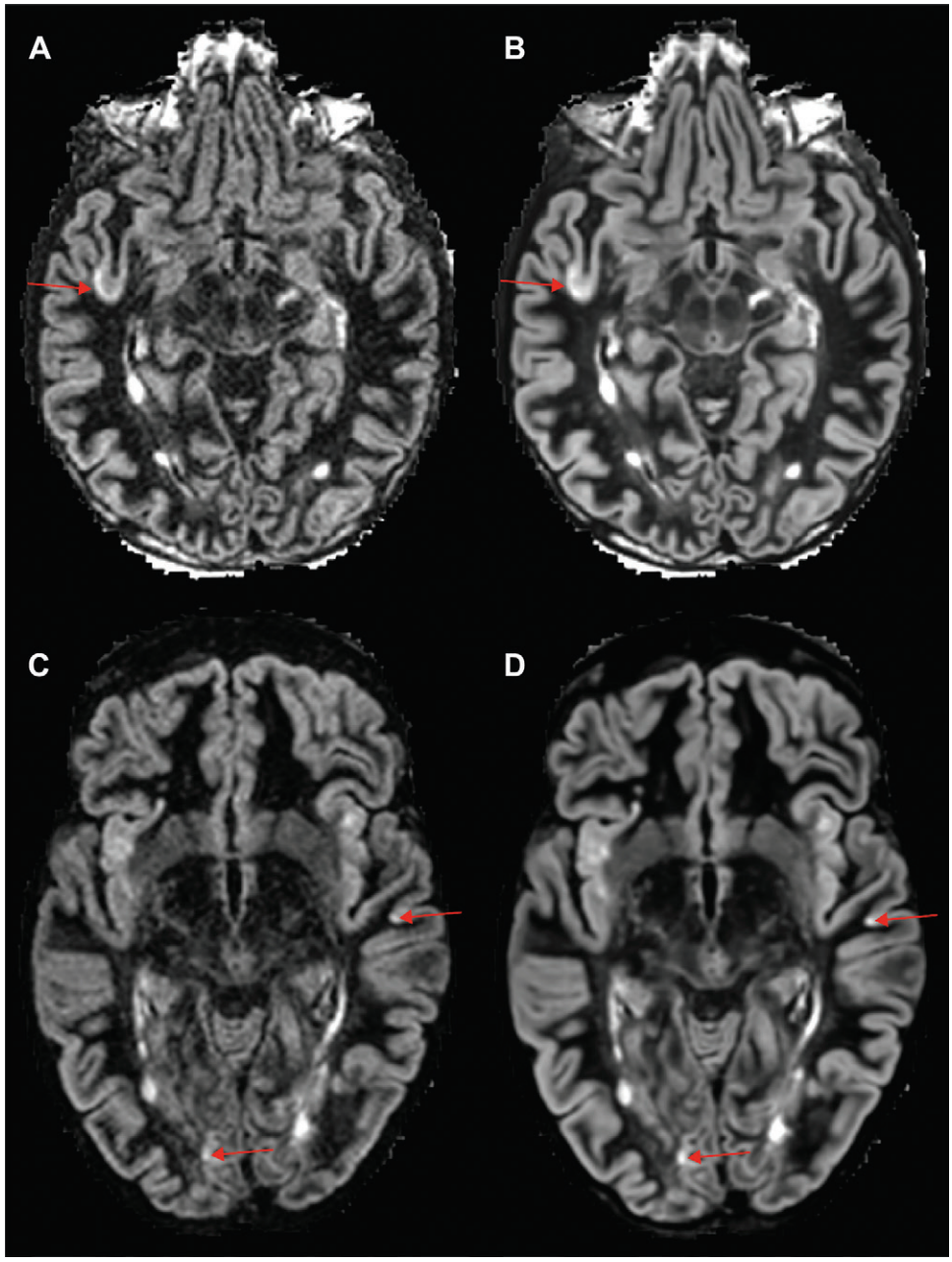

Figure 3: Examples of detected cortical lesions on axial double inversion-recovery (DIR) images. **(A, C)** MRI-acquired (noncontrast) and **(B, D)** artificial intelligence–generated DIR images. The arrows indicate detected intracortical lesions.

Our study suggests that a higher number of juxtacortical lesions can be detected on AI-generated DIR images than on MRI-acquired DIR images. This is different from earlier studies examining AI-generated DIR images, which found similar numbers of detected lesions (15,17). The higher number of detected lesions in the AI-generated DIR images was also reflected in the precision and may have emerged from the smoother appearance of the AI-generated images and the influence of AI on the cortical rim (due to white matter suppression optimization by the algorithm). This, in turn, might have influenced the differentiation between subcortical and juxtacortical lesions: Readers were specifically instructed to make this differentiation based on lesions touching (ie, juxtacortical) or not touching (ie, subcortical) the cortex. Of these, only juxtacortical lesions were to be annotated. Another explanation is the T1 component in the AI-generated images: T1-weighted images have previously been found to provide better contrast for juxtacortical lesions than T2-weighted images (21). However, the most important finding is that AI-generated DIR and PSIR images provide a tool for cortical lesion detection with which a similar number of cortical lesions can be detected compared with MRI-acquired DIR and PSIR images. These findings might contribute to diagnostic considerations for the establishment of dissemination in space and imaging protocols in multiple sclerosis care (9,11).

The results also showed high comparability between AI-generated and MRI-acquired PSIR images. Previous research found that PSIR may provide sharper contrast between gray and white matter compared with DIR and thereby enable the reader to distinguish more accurately between juxtacortical and leukocortical lesions (22). These findings seem to be reflected in our results,

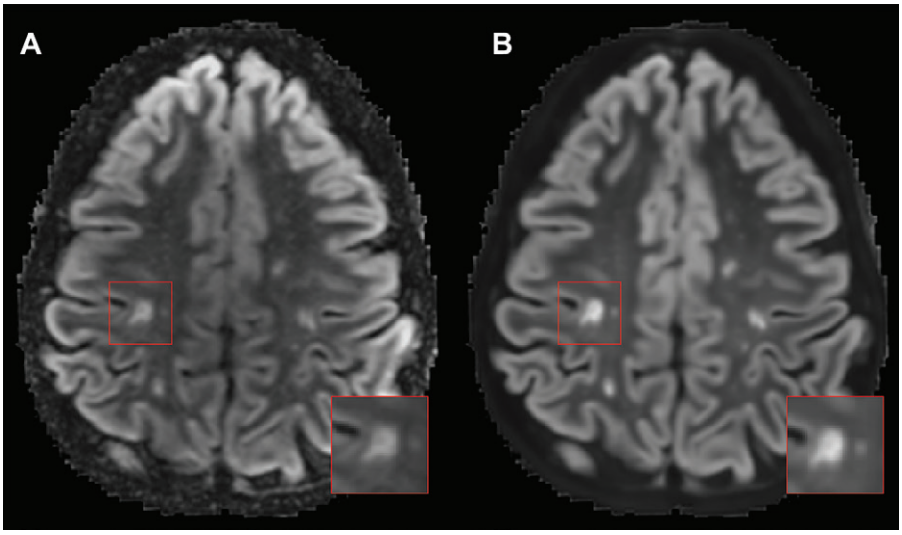

Figure 4: Example of a false-positive annotated lesion. **(A)** Axial MRI-acquired versus **(B)** artificial intelligence (AI)–generated double inversion-recovery images (noncontrast) in a 38-year-old woman. The inset indicates a lesion that was considered a juxtacortical lesion on the AI-generated image but was not identified as such on the MRI-acquired image due to the rim of white matter that is visible between the lesion and the cortex.

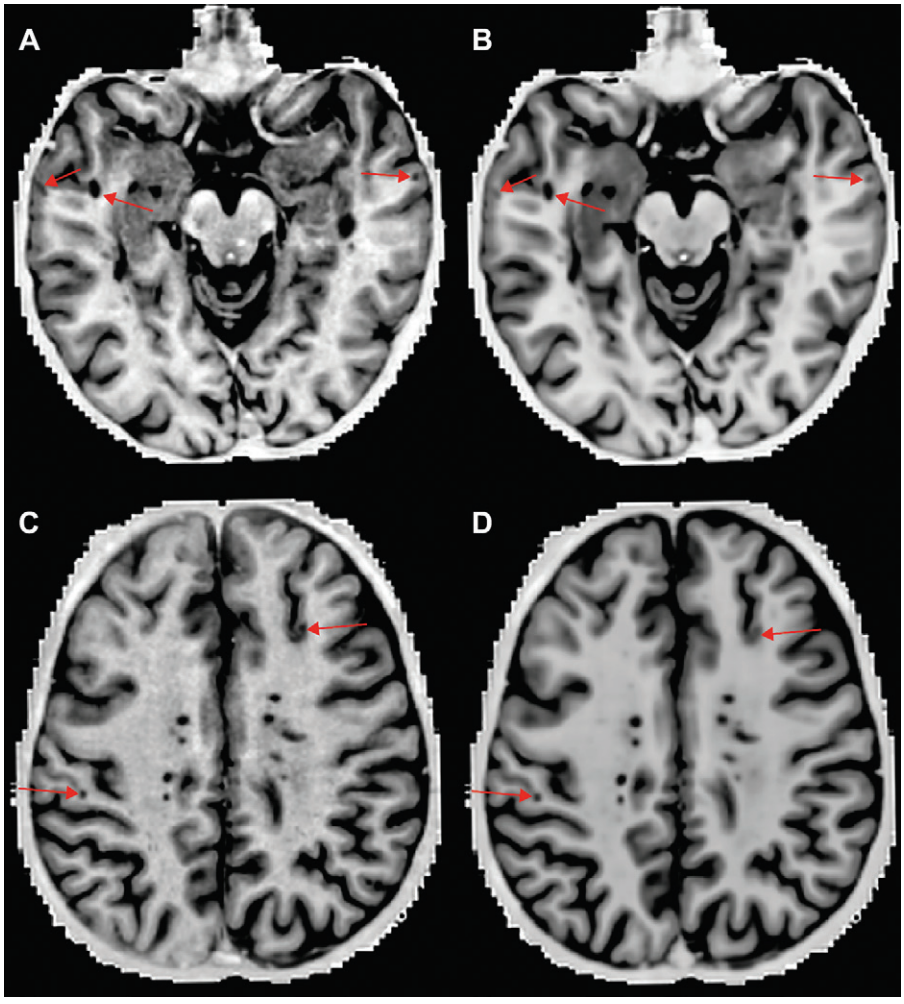

Figure 5: Overview of detected cortical lesions on axial phase-sensitive inversion-recovery (PSIR) images. **(A, C)** MRI-acquired versus **(B, D)** artificial intelligence–generated PSIR images. The arrows indicate detected intracortical and leukocortical lesions.

with more leukocortical than juxtacortical lesions detected on PSIR images. The precision of PSIR may have been reduced by false-positive findings, which were predominantly located infratentorially. This may be because T2-weighted sequences are preferred for infratentorial lesion assessment and because the AI-generated images contained a T2-weighted component. For both DIR and PSIR, the overall number of detected infratentorial lesions might have been underestimated, as three-dimensional fluid-attenuated inversion-recovery and T2-weighted spin-echo sequences are generally used for the detection of these lesions, rather than DIR or PSIR (9,23). Concordant with the previous literature, most of the detected lesions were situated in the temporal and frontal lobes (24–30). The location of the detected lesions may be relevant to unravel their role in, for example, physical or cognitive deterioration or disease progression and conversion (8,30–35). In regard to lesion detection on AI-generated PSIR images, studies are lacking in the literature. It is important, however, to note that our study does not postulate a direct comparison between AI-generated DIR and PSIR images, as different patients' images were assessed.

This study had limitations. First, regarding in vivo data, MRI-acquired images had to be used as reference rather than histopathologic findings. Although histopathologic validation of AI-generated DIR images yielded promising results (ie, 90% specificity), histopathologic validation of AI-generated PSIR images should be addressed in future endeavors (4,17). Second, 3-mm reformatting of the images increased the difficulty of assessing small suspect lesions (eg, distinguishing between lesions and cortical vessels or Virchow-Robin spaces). However, through-plane averaging might also have improved lesion discernibility in some instances. Third, the resolution of the coronal and sagittal images was not optimized, and thus, they could not be used for lesion detection or verification. Altogether, this may have hampered cortical lesion detection to some extent. However, all these impediments were present in both

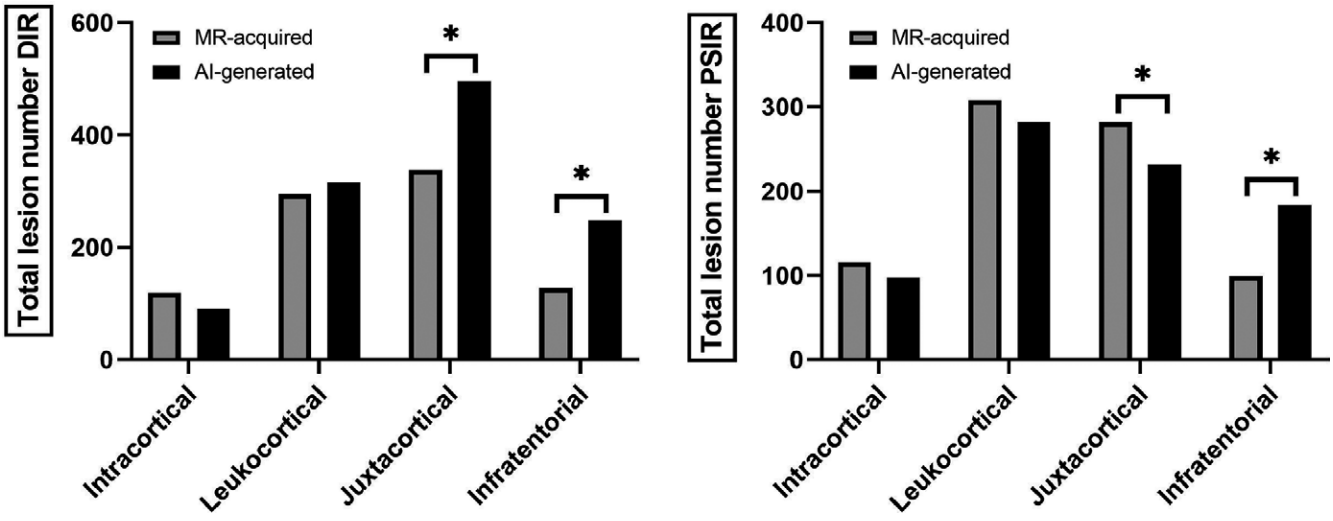

Figure 6: Bar graphs show the total number of detected lesions per lesion type. The left graph shows total lesion numbers that were detected on artificial intelligence (AI)–generated double inversion-recovery (DIR) images versus MRI-acquired DIR images per lesion subtype. The right graph shows an overview of total lesion numbers that were detected on AI-generated phase-sensitive inversion-recovery (PSIR) versus MRI-acquired PSIR images. * = $P < .05$.

Table 2: Contrast Ratios and Average ROI Size

Contrast	AI-generated DIR	MRI-acquired DIR	AI-generated PSIR	MRI-acquired PSIR
Contrast ratio				
CL-NAGM	0.23 ± 0.20	0.26 ± 0.23	−0.08 ± 0.12	−0.12 ± 0.07*
NAGM-NAWM	0.43 ± 0.16	0.51 ± 0.18*	−0.12 ± 0.08	−0.13 ± 0.08
Average ROI size (mm^2)				
CL-NAGM	50.8 ± 37.7	50.8 ± 37.7	37.4 ± 20.7	37.4 ± 20.7
NAGM-NAWM	48.8 ± 30.7	47.3 ± 25.8	37.1 ± 17.1	37.6 ± 17.2

Note.—Data are means ± SDs. The contrast ratio is calculated as [SI_1 (lesion/gray matter) – SI_2]/SI_2 (adjacent normal-appearing gray/white matter). Regions of interest (ROIs) were placed on lesions and adjacent normal-appearing white or gray matter. AI = artificial intelligence, CL-NAGM = cortical lesion to normal-appearing gray matter, DIR = double inversion recovery, NAGM-NAWM = normal-appearing gray matter to normal-appearing white matter, PSIR = phase-sensitive inversion recovery, SI = signal intensity.

* $P \leq .05$ compared with the AI-generated counterpart of a given sequence.

AI-generated and MRI-acquired images. Future endeavors should compare lesion detection numbers on a per-protocol basis to evaluate which combination of sequences (for different vendors and two- and three-dimensional acquisitions) would generate artificial images with the highest achievable detection potential.

In conclusion, our study showed that the number of detectable cortical and juxtacortical lesions on artificial intelligence (AI)–generated double inversion-recovery (DIR) and phase-sensitive inversion-recovery (PSIR) images is at least equal to their MRI-acquired counterparts. Not only were the images generated using multicenter input data, they were also assessed for cortical and juxtacortical lesions with good between-center and between-reader agreement. This indicates that AI-generated DIR and PSIR images can serve as a practical alternative to visualize cortical pathologic abnormalities in multiple sclerosis in clinical care or (retrospective) clinical studies when their MRI-acquired counterparts are desired but absent.

Author contributions: Guarantors of integrity of entire study, **P.M.B., J.J.G.G., M.D.S.**; study concepts/study design or data acquisition or data analysis/interpretation, all authors; manuscript drafting or manuscript revision for important intellectual content, all authors; approval of final version of submitted manuscript, all authors; agrees to ensure any questions related to the work are appropriately resolved, all authors; literature research, **P.M.B.**; clinical studies, **P.M.B., M. Castellaro, P.E., M.I., B.M., P.P., D.S.R., M.A.R., M.D.S.**; experimental studies, **P.M.B., S.N., E.S.B., G.B., M. Calabrese, D.T.C., M.I., C.L., A.M., P.P., L.E.J., C.R.G.G.**; statistical analysis, **P.M.B., J.W.R.T., L.E.J.**; and manuscript editing, **P.M.B., S.N., E.S.B., M. Castellaro, M. Calabrese, D.T.C., P.E., M.F., M.I., A.M., B.M., A.M.P., M.M., P.P., D.S.R., M.A.R., M.M.S., J.W.R.T., B.W., L.E.J., C.R.G.G., J.J.G.G., M.D.S.**

Disclosures of conflicts of interest: **P.M.B.** Support from Amsterdam UMC – VU University Amsterdam. **S.N.** No relevant relationships. **F.A.N.S.** No relevant relationships. **E.S.B.** Career transition award paid to institution from the National Multiple Sclerosis Society; patent pending for high-resolution cerebrospinal fluid–suppressed T2*-weighted MRI of cortical lesions. **G.B.** No relevant relationships. **M. Castellaro** No relevant relationships. **M. Calabrese** Grants to institution from Roche, Novartis, and Merck Serono; consulting fees from Roche, Novartis, Merck Serono, and Genzyme; payment for lectures from Roche, Novartis, Merck Serono, and Genzyme; support for attending meetings or travel from Roche, Novartis, and Merck Serono. **D.T.C.** Grants from F. Hoffmann-La Roche, the International Progressive MS Alliance, the MS Society, the Medical Research Council, and the National Institute for Health Research (NIHR) University College London Hospitals (UCLH) Biomedical Research Centre; consulting fees from F. Hoffmann-La Roche and Biogen; payment for lectures from Novartis; co-supervisor of a clinical fellowship at the National Hospital for Neurology and Neurosurgery, London, which is supported by Merck. **P.E.** No relevant relationships. **M.F.** Grants to institution from Biogen, Merck Serono, Novartis, Roche, the Italian Ministry of Health, Fondazione Italiana Sclerosi Multipla, and ARiSLA (Fondazione Italiana di Ricerca per la SLA); consulting fees

from Alexion, Almirall, Biogen, Merck, Novartis, Roche, and Sanofi; speaker honoraria from Bayer, Biogen, Celgene, Chiesi Italia, Eli Lilly, Genzyme, Janssen, Merck Serono, Neopharmed Gentili, Novartis, Novo Nordisk, Roche, Sanofi, Takeda, and Teva; scientific direction of educational events for Biogen, Merck, Roche, Celgene, Bristol Myers Squibb, Lilly, Novartis, and Sanofi Genzyme; participation on a data safety monitoring board or advisory board for Alexion, Biogen, Bristol Myers Squibb, Merck, Novartis, Roche, Sanofi, Sanofi-Aventis, Sanofi Genzyme, and Takeda; editor in chief of the *Journal of Neurology*, associate editor of *Human Brain Mapping*, associate editor of *Radiology*, and associate editor of *Neurological Sciences*. **M.I.** Consulting fees from Novartis, Roche, Merck, Almirall, Biogen, and Janssen; payment for lectures from Novartis, Roche, Merck, Almirall, Biogen, Janssen, and BMS. **C.L.** Payment for lectures from Novartis; support for attending meetings or travel from Merck and Roche. **A.M.** No relevant relationships. **B.M.** No relevant relationships. **A.M.P.** No relevant relationships. **M.M.** Grant to institution from the German Research Foundation (DFG SPP2177). **P.P.** Research support to institution from the Italian Ministry of Health and Fondazione Italiana Sclerosi Multipla; speaker honoraria from Roche, Biogen, Novartis, Merck Serono, Bristol Myers Squibb, and Genzyme. **D.S.R.** Grants to institution from Abata Therapeutics, Sanofi, and Vertex; payment for expert testimony from Bounds Law Group; patent pending for high-resolution cerebrospinal fluid–suppressed T2*-weighted MRI of cortical lesions and patent issued for automatic identification of subjects at risk of multiple sclerosis. **M.A.R.** Grants to institution from the MS Society of Canada and the Fondazione Italiana Sclerosi Multipla; consulting fees from Biogen, Bristol Myers Squibb, Eli Lilly, Janssen, and Roche; speaker honoraria from Bayer, Biogen, Bristol Myers Squibb, Bromatech, Celgene, Genzyme, Merck Healthcare Germany, Merck Serono, Novartis, Roche, and Teva; associate editor for *Multiple Sclerosis and Related Disorders*. **M.M.S.** Grants to institution from the Dutch MS Research Foundation, Eurostars-EUREKA, ARSEP, Amsterdam Neuroscience, Magnetic Resonance Imaging in MS (MAGNIMS), ZonMw, Atara Biotherapeutics, Biogen, Celgene/Bristol Myers Squibb, Sanofi Genzyme, and Merck; speaker fees to institution from Excellence in Medical Education and Sanofi Genzyme; unpaid board member of MS Center Amsterdam, head of the International Multiple Sclerosis Cognition Society steering committee, and editorial board member of *Neurology*, *Frontiers in Neurology*, and *Radiology*. **J.W.R.T.** No relevant relationships. **B.W.** Grants from the German Research Foundation (DFG) and SPP Radiomics; speaker honorarium from Philips. **L.E.J.** Grants to institution from the Michael J. Fox Foundation, Alzheimer Nederland Stichting Parkinson Fonds, Health~Holland TKI, and the Alzheimer's Association; support for travel from the Alzheimer's Association International Conference. **C.R.G.G.** No relevant relationships. **J.J.G.G.** No relevant relationships. **M.D.S.** No relevant relationships.

References

1. Amato MP, Zipoli V, Portaccio E. Multiple sclerosis-related cognitive changes: a review of cross-sectional and longitudinal studies. J Neurol Sci 2006;245(1-2):41–46.
2. Compston A, Coles A. Multiple sclerosis. Lancet 2008;372(9648):1502–1517.
3. Reich DS, Lucchinetti CF, Calabresi PA. Multiple sclerosis. N Engl J Med 2018;378(2):169–180.
4. Bouman PM, Steenwijk MD, Pouwels PJW, et al. Histopathology-validated recommendations for cortical lesion imaging in multiple sclerosis. Brain 2020;143(10):2988–2997.
5. Seewann A, Kooi EJ, Roosendaal SD, et al. Postmortem verification of MS cortical lesion detection with 3D DIR. Neurology 2012;78(5):302–308.
6. Seewann A, Vrenken H, van der Valk P, et al. Diffusely abnormal white matter in chronic multiple sclerosis: imaging and histopathologic analysis. Arch Neurol 2009;66(5):601–609.
7. Geurts JJG, Barkhof F. Grey matter pathology in multiple sclerosis. Lancet Neurol 2008;7(9):841–851.
8. Calabrese M, Agosta F, Rinaldi F, et al. Cortical lesions and atrophy associated with cognitive impairment in relapsing-remitting multiple sclerosis. Arch Neurol 2009;66(9):1144–1150.
9. Filippi M, Preziosa P, Banwell BL, et al. Assessment of lesions on magnetic resonance imaging in multiple sclerosis: practical guidelines. Brain 2019;142(7):1858–1875.
10. Rovira À, Wattjes MP, Tintoré M, et al; MAGNIMS study group. Evidence-based guidelines: MAGNIMS consensus guidelines on the use of MRI in multiple sclerosis-clinical implementation in the diagnostic process. Nat Rev Neurol 2015;11(8):471–482.
11. Thompson AJ, Banwell BL, Barkhof F, et al. Diagnosis of multiple sclerosis: 2017 revisions of the McDonald criteria. Lancet Neurol 2018;17(2):162–173.
12. Seewann A, Vrenken H, Kooi EJ, et al. Imaging the tip of the iceberg: visualization of cortical lesions in multiple sclerosis. Mult Scler 2011;17(10):1202–1210.
13. Geurts JJG, Pouwels PJW, Uitdehaag BMJ, Polman CH, Barkhof F, Castelijns JA. Intracortical lesions in multiple sclerosis: improved detection with 3D double inversion-recovery MR imaging. Radiology 2005;236(1):254–260.
14. Sethi V, Yousry TA, Muhlert N, et al. Improved detection of cortical MS lesions with phase-sensitive inversion recovery MRI. J Neurol Neurosurg Psychiatry 2012;83(9):877–882.
15. Bouman PM, Strijbis VIJ, Jonkman LE, Hulst HE, Geurts JJG, Steenwijk MD. Artificial double inversion recovery images for (juxta)cortical lesion visualization in multiple sclerosis. Mult Scler 2022;28(4):541–549.
16. Finck T, Li H, Grundl L, et al. Deep-learning generated synthetic double inversion recovery images improve multiple sclerosis lesion detection. Invest Radiol 2020;55(5):318–323.
17. Bouman PM, Steenwijk MD, Geurts JJG, Jonkman LE. Artificial double inversion recovery images can substitute conventionally acquired images: an MRI-histology study. Sci Rep 2022;12(1):2620.
18. Polman CH, Reingold SC, Banwell B, et al. Diagnostic criteria for multiple sclerosis: 2010 revisions to the McDonald criteria. Ann Neurol 2011;69(2):292–302.
19. Poser CM, Paty DW, Scheinberg L, et al. New diagnostic criteria for multiple sclerosis: guidelines for research protocols. Ann Neurol 1983;13(3):227–231.
20. Geurts JJG, Roosendaal SD, Calabrese M, et al; MAGNIMS Study Group. Consensus recommendations for MS cortical lesion scoring using double inversion recovery MRI. Neurology 2011;76(5):418–424.
21. Beck ES, Sati P, Sethi V, et al. Improved visualization of cortical lesions in multiple sclerosis using 7T MP2RAGE. AJNR Am J Neuroradiol 2018;39(3):459–466.
22. Sethi V, Muhlert N, Ron M, et al. MS cortical lesions on DIR: not quite what they seem? PLoS One 2013;8(11):e78879.
23. Gabr RE, Lincoln JA, Kamali A, et al. Sensitive detection of infratentorial and upper cervical cord lesions in multiple sclerosis with combined 3D FLAIR and T2-weighted (FLAIR3) imaging. AJNR Am J Neuroradiol 2020;41(11):2062–2067.
24. Bagnato F, Butman JA, Gupta S, et al. In vivo detection of cortical plaques by MR imaging in patients with multiple sclerosis. AJNR Am J Neuroradiol 2006;27(10):2161–2167.
25. Brownell B, Hughes JT. The distribution of plaques in the cerebrum in multiple sclerosis. J Neurol Neurosurg Psychiatry 1962;25(4):315–320.
26. Calabrese M, Battaglini M, Giorgio A, et al. Imaging distribution and frequency of cortical lesions in patients with multiple sclerosis. Neurology 2010;75(14):1234–1240.
27. Calabrese M, Filippi M, Gallo P. Cortical lesions in multiple sclerosis. Nat Rev Neurol 2010;6(8):438–444.
28. Favaretto A, Lazzarotto A, Poggiali D, et al. MRI-detectable cortical lesions in the cerebellum and their clinical relevance in multiple sclerosis. Mult Scler 2016;22(4):494–501.
29. Filippi M, Rocca MA, Calabrese M, et al. Intracortical lesions: relevance for new MRI diagnostic criteria for multiple sclerosis. Neurology 2010;75(22):1988–1994.
30. Roosendaal SD, Moraal B, Pouwels PJW, et al. Accumulation of cortical lesions in MS: relation with cognitive impairment. Mult Scler 2009;15(6):708–714.
31. Bagnato F, Salman Z, Kane R, et al. T1 cortical hypointensities and their association with cognitive disability in multiple sclerosis. Mult Scler 2010;16(10):1203–1212.
32. Calabrese M, Poretto V, Favaretto A, et al. Cortical lesion load associates with progression of disability in multiple sclerosis. Brain 2012;135(Pt 10):2952–2961.
33. Geurts JJG, Calabrese M, Fisher E, Rudick RA. Measurement and clinical effect of grey matter pathology in multiple sclerosis. Lancet Neurol 2012;11(12):1082–1092.
34. Haider L, Prados F, Chung K, et al. Cortical involvement determines impairment 30 years after a clinically isolated syndrome. Brain 2021;144(5):1384–1395.
35. Rinaldi F, Calabrese M, Grossi P, Puthenparampil M, Perini P, Gallo P. Cortical lesions and cognitive impairment in multiple sclerosis. Neurol Sci 2010;31(Suppl 2):S235–S237.